Available online at www.sciencedirect.com
ScienceDirect
Journal of Power Sources 171 (2007) 55–62
JOURNAL OF POWER SOURCES
www.elsevier.com/locate/jpowsour

High performance of low electrocatalysts loading on CNT directly grown on carbon cloth for DMFC

C.-H. Wang [a], H.-Y. Du [b], Y.-T. Tsai [b], C.-P. Chen [c], C.-J. Huang [b], L.C. Chen [c], K.H. Chen [c,d,*], H.-C. Shih [a,b,**]

[a] *Department of Materials Science and Engineering, National Tsing Hua University, Hsinchu 30013, Taiwan*
[b] *Institute of Materials Science and Nano Technology, Chinese Culture University, Taipei 11114, Taiwan*
[c] *Center for Condensed Matter Sciences, National Taiwan University, Taipei 10617, Taiwan*
[d] *Institute of Atomic and Molecular Science, Academia Sinica, Taipei 10617, Taiwan*

Received 12 September 2006; received in revised form 26 November 2006; accepted 11 December 2006
Available online 28 December 2006

Abstract

This study demonstrated the feasibility of a high-performance membrane-electrode-assembly (MEA), with low electrocatalyst loading on carbon nanotubes (CNTs) grown directly on carbon cloth as an anode. The direct growth of CNTs was synthesized by microwave plasma-enhanced chemical vapor deposition using $CH_4/H_2/N_2$ as precursors. The cyclic voltammetry and electrochemical impedance measurements with 1 mM $Fe(CN)_6^{3-/4-}$ redox reaction reveal a fast electron transport and a low resistance of charge transfer on the direct growth of CNT. The electrocatalysts, platinum and ruthenium, were coated on CNTs by sputtering to form Pt-Ru/CNTs-CC with carbon cloth for CC. Pt-Ru electrocatalysts are uniformly dispersed on the CNT, as indicated by high-resolution scanning electron microscopy (HRSEM) and transmission electron microscopy (TEM), because the nitrogen doped in the CNT acts as active sites for capturing electrocatalysts. The MEA, the sandwiched structure which comprises 0.4 mg cm^{-2} Pt-Ru/CNTs-CC as the anode, 3.0 mg cm^{-2} Pt black as the cathode and Nafion 117 membrane at the center, performs very well in a direct methanol fuel cell (DMFC) test. The micro-structural MEA analysis shows that the thin electrocatalyst layer is uniform, with good interfacial continuity between membrane and the gas diffusion layer.

Keywords: Fuel cell; Carbon nanotubes; Methanol oxidation; Nanocomposite; Direct growth

1. Introduction

The direct methanol fuel cell (DMFC) is an attractive and promising power generator with a wide range of applications from small sensors and portable electronic devices up to automobiles [1–3]. The DMFC directly consumes liquid fuel (methanol) and air, without the need for humidification, a thermal management system, a fuel vaporizer or reformer. The use of liquid methanol as fuel provides high energy density and convenient refueling. Indeed, methanol is regarded by some as critical to transport and compatibility with the current petroleum distribution network.

Membrane-electrode-assembly (MEA), a key component of DMFC, is a five-layer structure, which comprise gas diffusion layers (GDL, carbon cloth or carbon paper), electrocatalyst layers and a sandwiched Nafion® membrane [4]. The membrane is at the center and separates the electrodes (anode and cathode) to prevent mixing of the reactant gas and electrical shorting. Each electrode includes a GDL with the platinum-based electrocatalyst layer between the membrane and the GDL. In fabricating the optimal electrode, various parameters, including the composition of the catalyst itself, electrocatalyst loading, ionomer content in the catalyst layer, porosity of the electrode and others, must be investigated [5]. The methanol oxidation is regarded as a slow step in the overall redox reaction.

* Corresponding author at: Institute of Atomic and Molecular Science, Academia Sinica, Taipei 10617, Taiwan. Tel.: +886 2 2366 8232; fax: +886 2 2362 0200.
** Corresponding author at: Department of Materials Science and Engineering, National Tsing Hua University, Hsinchu 30013, Taiwan. Tel.: +886 2 2366 8232; fax: +886 2 2362 0200.
E-mail addresses: chenkh@pub.iams.sinica.edu.tw (K.H. Chen), hcshih@mx.nthu.edu.tw (H.-C. Shih).

0378-7753/$ – see front matter © 2006 Elsevier B.V. All rights reserved.
doi:10.1016/j.jpowsour.2006.12.028

Therefore, nanosized high-efficiency electrocatalysts (Pt-Ru) uniformly dispersed on a conductive carbon support (activated carbon) have been demonstrated to improve methanol oxidation [2,6–10].

In most of the published works, the Pt loading of anode is mostly above 1.0 mg cm^{-2} to ensure high methanol reactivity and to prevent methanol crossover to the cathode [11,12]. However, the associated cost is too high to allow the commercialization of the DMFC. In the MEA, the anode performance appears to be related to many factors, such as electrocatalysts utilization, the extent of the electrocatalysts/ionomer interface, the thickness of the electrocatalyst layer and the porosity. Increasing the weight percentage of Pt-Ru in the electrocatalyst layer reduces the thickness of the electrocatalyst layer, which can efficiently reduce mass transport resistance. However, the trade-off with metallic agglomeration also reduces the electrochemical reaction area [13–15].

In the fabrication of an efficient electrode, carbon nanotubes (CNTs), with a high conductivity, high surface area and corrosion resistance, have been thought to be a good electrocatalytic supports for electrochemical applications [16–21]. Electrocatalysts supported on multi-walled CNTs (MWNTs), single-walled CNTs (SWNT) or carbon nanofibers as electrodes in either proton exchange membrane fuel cells (PEMFCs) or DMFCs have been examined extensively [22–30]. They showed that electrocatalysts were uniformly dispersed on CNT, and their performance was improved by improving the properties of CNT. Recently, Tsai et al. showed that CNTs were directly grown on carbon cloth using thermal chemical vapor deposition under a gas mixture of C_2H_4/NH_3/Ar, and Pt-Ru were subsequently electrodeposited on CNTs in ethylene glycol containing H_2SO_4 aqueous solution [31]. Their results showed that the mass activity of Pt-Ru on directly grown CNT is higher than that of Pt-Ru/CC in methanol containing H_2SO_4 aqueous solution. Therefore, they concluded that this new arrangement would improve the electrical contact between the support and the diffusion layer and could avoid an undesirable decrease in active surface area from conventional catalyst pasting process. However, further information of the impedance analysis and the DMFC tests were absent.

This work attempts to fabricate an efficient CNT-based electrode tailored for DMFC, which minimizes electrocatalyst loading and maximizes electrocatalyst utilization. The nitrogen-doped CNT is directly grown on the carbon cloth as a template and then Pt-Ru electrocatalysts are dispersed on it. Accordingly, the DMFC performs well even with very low electrocatalyst loading of the anode.

2. Experimental

The CNTs directly grown on the carbon cloth (CNTs-carbon cloth composite electrode) were prepared by iron-assisted catalytic growth in a microwave plasma-enhanced chemical vapor deposition (MPECVD) reactor. The carbon cloth (Designation A, E-TEK) comprises carbon fibers with a diameter of 5–10 μm. A three dimensional network structure is formed from randomly arranged and bonded carbon fibers. The thickness and surface resistivity of the carbon cloth are 0.35 mm and 0.30 Ω $\square^{-1}$, respectively. The iron was sputtered on the carbon cloth as a catalyst layer by ion beam sputtering deposition to grow CNTs on the carbon cloth. The working pressure was maintained at 5×10^{-4} Torr in an atmosphere of argon during deposition and a Kaufman ion source was operated at a beam voltage of 1250 V and a current of 20 mA. The deposition time of the iron catalyst layer was 10 min. Following deposition, carbon cloth coated with an iron catalyst layer was then introduced to MPECVD. The hydrogen plasma treatment was operated at 1 kW and a chamber pressure of 28 Torr for 10 min. In this step, the iron catalyst layer was transformed into nanoparticles. Hydrogen plasma treatment not only reduced the iron oxides on the surface of the iron catalyst layer to the iron metal state but also generated more active catalyst sites. The CNTs were grown in a gas mixture of $H_2/CH_4/N_2$ (80:20:80) at a microwave power of 2 kW, a chamber pressure of 45 Torr and a substrate temperature of 900 °C for 10 min. In the preparation of electrocatalysts supported on the CNTs-carbon cloth composite electrode, physical vapor deposition (PVD) was adopted to sputter platinum and ruthenium on the template to form Pt-Ru/CNTs-CC electrode. For comparison, the electrocatalysts were also sputtered on a carbon cloth without CNTs treatment, namely, Pt-Ru/CC. The platinum and ruthenium targets were placed inside the radio-frequency planar magnetron sputtering guns in a PVD system. The deposition procedure was conducted in an argon atmosphere at a working pressure of 5×10^{-2} Torr. The holder rotates at a constant speed (20 rpm) during deposition to yield a highly uniform coating of Pt-Ru nanoclusters on CNTs.

The atomic ratio and mass per unit area of the metals were determined by electron spectroscopy for chemical analysis (ESCA, Perkin-Elmer model PHI 1600) and inductively coupled plasma-optical emission spectroscopy (ICP-OES, Perkin-Elmer ICP-OES Optima 3000), respectively. Transmission electron microscopy (TEM, JOEL-2000FX) and high-resolution scanning electron microscopy (HRSEM, JEOL-6700) were adopted to explore the surface morphologies and micro-structures of the electrodes. The crystal structure of the electrocatalysts was investigated using an X-ray diffraction (XRD, PANalytical X' Pert PRO diffractometer system with Cu Kα radiation at 1.54056 Å).

Electrochemical measurements and AC impedance analysis were conducted in a three-electrode test cell at room temperature using a Solartron electrochemical test system (SI 1280Z). The sample was put into a specific holder as a working electrode, which was connected to the test system with a golden wire. A 3 M KCl Ag/AgCl electrode was the reference electrode and a platinum foil served as the counter electrode. The potentials reported in this three-electrode test cell were with respect to 3 M KCl Ag/AgCl (0.207 V versus SHE). All solutions were degassed using high purity nitrogen and the cyclic voltammetry (CV) data were recorded until the CV scans remained constant.

The membrane-electrode-assembly was prepared by hot-pressing two electrodes on both sides of a Nafion® 117 (H^+, DuPont) at 135 °C and 130 kg cm^{-2} for 2 min. In the preparation of specific anodes, the Pt-Ru/CNTs-CC and the Pt-Ru/CC was immersed in 5 wt.% commercial Nafion® solution for 10 min.

In the preparation of conventional anodes, the catalyst ink, Pt-Ru supported by Vulcan XC-72 carbons (40 wt.% Pt and 20 wt.% Ru, Johnson Matthey) mixing with Nafion® solution and ethylene glycol, was applied to carbon cloth by screen-printing to form Pt-Ru/XC/CC electrode. The metal loadings on Pt-Ru/CNTs-CC, Pt-Ru/CC and Pt-Ru/XC/CC electrodes are 0.4, 0.4 and 3.0 mg cm^{-2}, respectively. The atomic ratio of Pt: Ru is 1:1 for all anodes. Commercial gas diffusion electrodes (3.0 mg cm^{-2} Pt black, E-TEK) were adopted as cathodes in MEAs. The polarization experiments were conducted with 1 M methanol pumped through the anode at a rate of 40 ml min^{-1} and pure O_2 flowed into the cathode at a rate of 400 standard cubic centimeters per minute (SCCM). The cell performance was measured using a DMFC test station (Asia Pacific Fuel Cell Technologies Ltd.) by recording the cell voltage and current after they had reached a steady value.

3. Results and discussion

Fig. 1 presents the HRSEM image of the overall configuration of the non-directional CNTs on conductive carbon fibers. The diameter of the CNTs is approximately 20 nm, as shown in the inset of Fig. 1. The length of CNTs varies markedly between 5 and 10 μm. The iron catalysts promote the growth of CNTs, and the figure clearly shows that CNTs nucleate and grow well on the carbon cloth. Most iron catalysts are trapped on the outer carbon fibers of the carbon cloth, where in the CNTs grow. The morphology of CNTs grown on the carbon cloth depends much on the processing details. Fig. 2(a) displays a cross-sectional TEM image of iron coated on a carbon cloth in the early stage of growth, subject to treatment with hydrogen plasma. Notably, the amorphous carbon film encapsulates iron nanoparticles. When no external carbon source is introduced in this early stage, high-energy ions and free radicals in the hydrogen plasma bombard carbon fibers and generated some hydrocarbon ions or radicals. These hydrocarbon ions or radicals may be deposited as the amorphous carbon film and then the iron catalyst is encapsulated. The iron catalyst is assumed to induce the formation of amorphous carbon film on itself, and

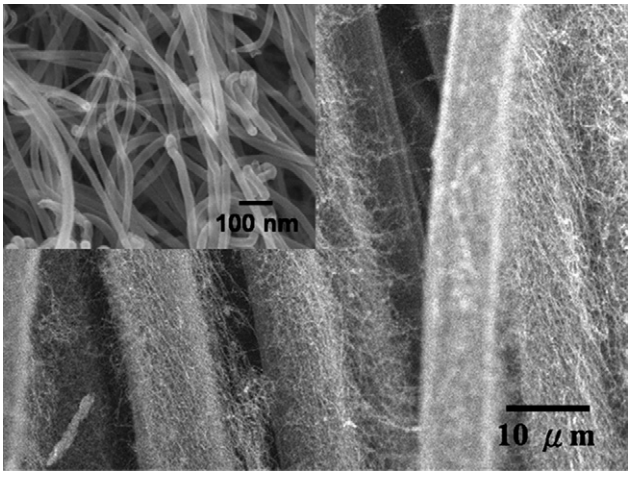

Fig. 1. HRSEM showing the CNTs directly grown on carbon cloth.

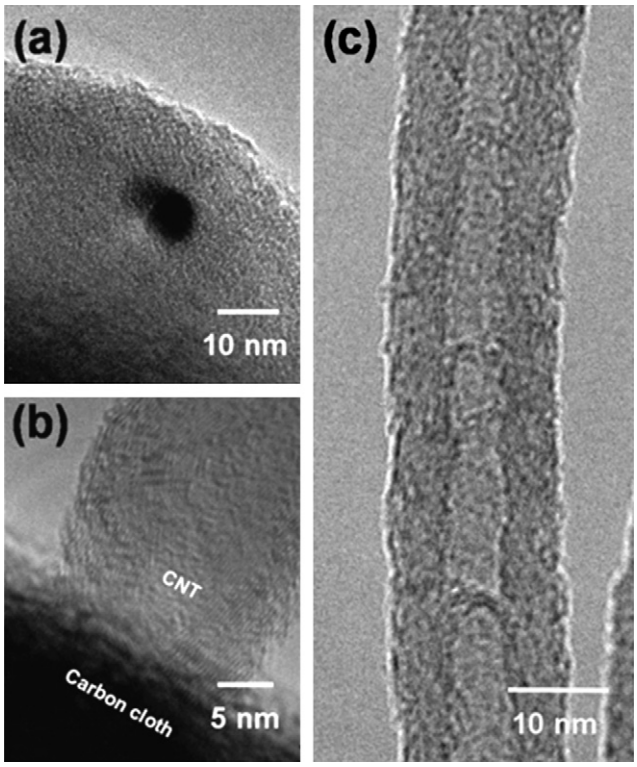

Fig. 2. TEM images showing (a) the iron catalyst encapsulated in amorphous carbon film at early stage of growth, (b) the cross-sectional view of CNTs directly conjoin with carbon cloth and (c) the micro-structural CNT.

this film promotes the subsequent growth of CNT [32]. Fig. 2(b) presents a cross-sectional TEM image of the CNT that is grown directly on carbon cloth. The image reveals that the graphene sheets of CNT not only adhere to the carbon cloth but also directly conjoined with the carbon cloth. Fig. 2(c) shows that the sample is a multi-walled carbon nanotube with a bamboo-like structure. The nitrogen in CNTs is approximately 8%, as revealed by EDX. Adding N_2 to the process gas is believed to promote the formation of a bamboo-like structure with a surface with high curvature [32–35]. The bonding of nitrogen atoms in a solid-state network is inherently non-planar in the presence of a lone pair of electrons, whereas sp^2 bonding of the carbon atom is typically planar. Furthermore, the incorporation of nitrogen atoms into graphene sheets with a bamboo-like structure favor the formation of pentagons and heptagons, and increase the reactivity of the neighboring carbon atoms, yielding decorated nanotubes. These substituted nitrogen sites may be the initial nucleation sites of the deposition of Pt-Ru nanoparticles. Rajesh et al. demonstrated that 3–8% nitrogen incorporated in CNT increases methanol oxidation activity, and they conjectured that nitrogen-doped CNTs could improve the dispersion of the catalytic nanoparticles [36].

The redox reaction of $Fe(CN)_6^{3-/4-}$ was used as an electrochemical benchmark to examine various electrodes. Fig. 3(a) plots the CV measurements of a CNTs-carbon cloth composite electrode and a carbon cloth in 1 mM potassium ferricyanide and 1 M sulfuric acid solution obtained at a scan rate of 50 mV s^{-1}. Clearly, the anodic and cathodic peak current densities ($I_{p,a}$

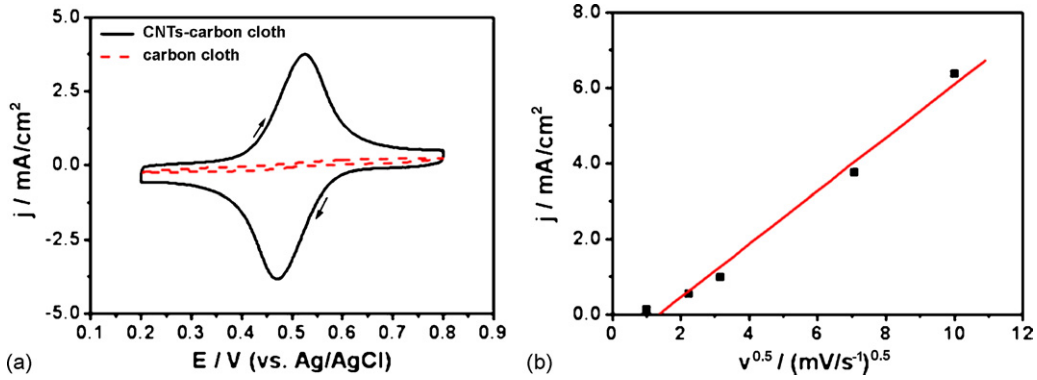

Fig. 3. (a) CV measurements for the CNTs-carbon cloth composite electrode and the carbon cloth in 1 mM $K_3Fe(CN)_6$/1 M H_2SO_4 at a scan rate of 50 mV s^{-1} and (b) the relation of anodic peak current densities vs. square root of scan rate for the CNTs-carbon cloth composite electrode.

and $I_{p,c}$) of the CNTs-carbon cloth composite electrode considerably exceed those of the carbon cloth. Furthermore, the separation between anodic and cathodic peak potentials ($E_{p,a}$ and $E_{p,c}$) is 60 mV, indicating that nearly reversible redox reaction occurs on the CNTs-carbon cloth composite electrode. Fig. 3(b) plots $I_{p,a}$ versus the square root of scan rate (v) for the CNTs-carbon cloth composite electrode, and the linear relationship demonstrates that the redox reaction is diffusion-controlled on the CNTs-carbon cloth composite electrode. A larger reaction area and faster electron transfer on the CNTs-carbon cloth composite electrode may be responsible for the higher performance of redox reactions [37–39]. Electrochemical impedance spectroscopy (EIS), which is the ac impedance as a function of the frequency of ac sources, is measured to study the conductivity and charge transport behaviors of electrodes. Impedance spectra at the steady-state potential were obtained with an amplitude of 10 mV from 20 kHz to 1 Hz. Fig. 4(a and b) shows Nyquist plots of the CNTs-carbon cloth composite electrode and the carbon cloth at 0.6 V. The impedance spectrum of the CNTs-carbon cloth composite electrode clearly differs from that of the carbon cloth. The Nyquist plot of the CNTs-carbon cloth composite electrode has a depressed semi-circle in the high-frequency region and a straight line in the low frequency region. The depressed semi-circle at high-frequency is attributed to the Faradaic process of charge exchange at the electrode/electrolyte interfaces, and the straight line at low frequency can be understood using a finite-length Warburg element. The Nyquist plot of the carbon cloth shows very high impedances, and it is a depressed semi-circle in the all-frequency region, which is consistent with the well-known Randles circuit model in which the Warburg impedance is unimportant [40].

Fig. 4(c and d) presents the equivalent-circuit models for the CNTs-carbon cloth composite electrode and carbon cloth, respectively. The figures can be explained by the impedance behaviors. In these models, R_s and R_{ct} are the solution resistance and the charge-transfer resistance, respectively. The double-layer capacitance is substituted by the constant phase element (CPE) in the circuit, which is

$$Z_{CPE} = \frac{1}{C(j\omega)^a} \quad (1)$$

where C is the admittance constant, a an adjustment parameter and ω is the frequency [41]. Z_w is a finite-length Warburg

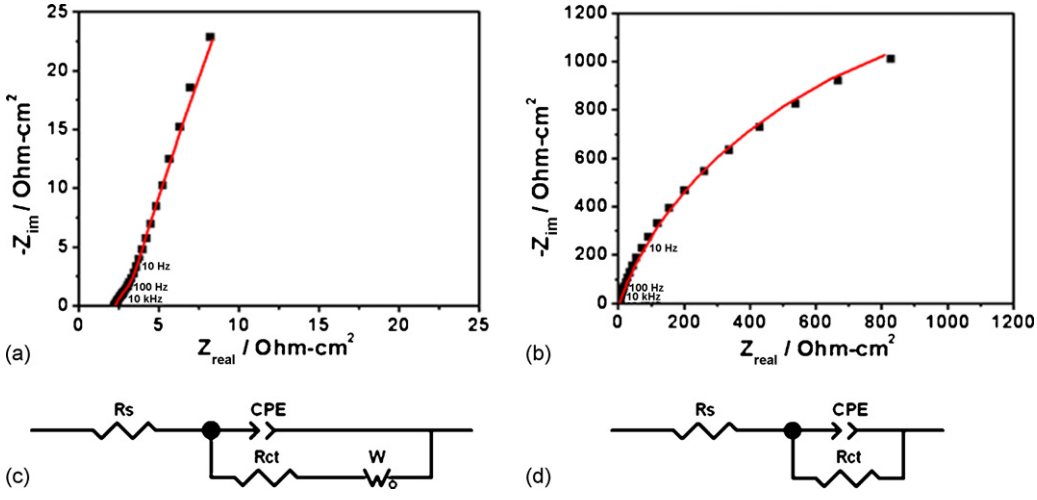

Fig. 4. Nyquist plots (dots) and the fitting lines (solid lines) of (a) the CNTs-carbon cloth composite electrode and (b) the carbon cloth in 1 mM $K_3Fe(CN)_6$/1 M H_2SO_4; the equivalent-circuit models of (c and d) for fitting (a and b), respectively.

Table 1
Fitted parameters for CNTs-carbon cloth electrode and carbon cloth in 1 mM $K_3Fe(CN)_6$/1 M H_2SO_4

	R_s (Ω cm^2)	$C \times 10^5$ (Ω^{-1} s^a cm^{-2})	a	R_{ct} (Ω cm^2)	W (Ω cm^2)	T (s)
CNTs-CC	2.252	751.6	0.79	0.46	16.55	0.0285
Carbon cloth	2.240	13.2	0.84	3121	–	–

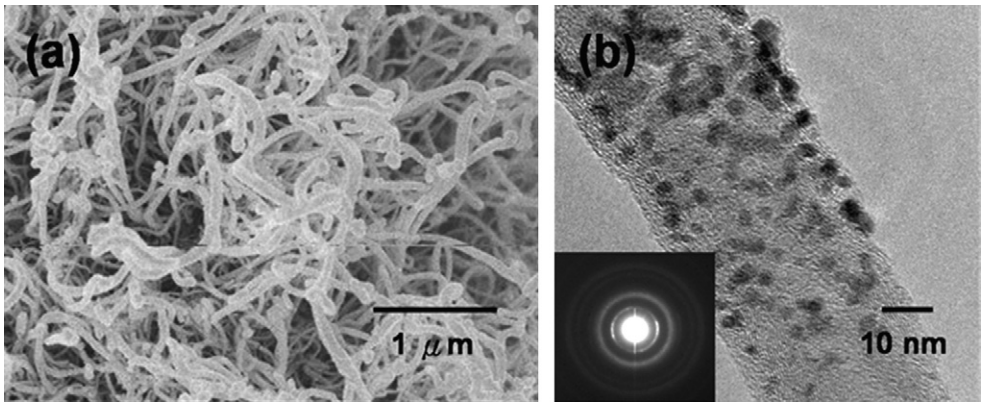

Fig. 5. Pt-Ru electrocatalysts on the CNTs-carbon cloth composite electrode: (a) HRSEM image and (b) TEM image with a SAD pattern in the inset.

impedance at a reflective boundary, which is given by,

$$Z_w = W \times \frac{\coth(j \times T \times \omega)^{0.5}}{(j \times T \times \omega)^{0.5}} \quad (2)$$

where W is the admittance constant and T is the square of the effective diffusion thickness divided by the effective diffusion coefficient. This finite-length Warburg impedance corresponds to diffusion into a layer of electrolyte or active material with limited thickness [41]. The corresponding solid lines in Fig. 4(a and b) plot the fitting results based on the equivalent-circuit models in Fig. 4(c and d), respectively, and the fitted parameters are listed in Table 1. The fitted parameters in Table 1 indicate that the double-layer capacitance of CNTs-carbon cloth composite electrode is substantially higher than that of carbon cloth, and the charge-transfer resistance (R_{ct}) and the following Warburg impedance (Z_w) of CNTs-carbon cloth composite electrode are significantly lower than those of carbon cloth. In support of CV and EIS analyses, the CNTs-carbon cloth composite electrode is established to support faster electron transport and a lower charge-transfer resistance.

High surface area and nanoscale of Pt-Ru electrocatalysts demonstrate the best performance to date as methanol oxidation electrocatalysts in the DMFC [42]. The enhanced activity of Pt-Ru electrocatalysts has been attributed to both bi-functional mechanism [43] and ligand effect [44]. Fig. 5(a) shows the HRSEM image of Pt-Ru electrocatalysts deposited on a CNTs-carbon cloth composite electrode by sputtering. A TEM image (Fig. 5(b)) presents homogeneously dispersed Pt-Ru nanoclusters on the surface of CNT. Since the incorporation of nitrogen in CNT promotes the dispersion of nanoparticles on the surface [45,46], it is also associated with highly uniform Pt-Ru nanoclusters dispersed on CNT in this case, as presented in Fig. 5(b). The rings in the corresponding selected area diffraction (SAD) pattern, displayed in the inset in Fig. 5(b), demonstrate that the Pt-Ru nanoclusters are polycrystalline and randomly oriented.

Fig. 6 shows the X-ray diffraction patterns measured on the Pt-Ru/CNTs-CC, the Pt-Ru/CC and the Pt-Ru/XC/CC, as well as the background pattern of the carbon cloth. Three samples exhibit only the characteristic diffraction peaks of the fcc structure of platinum at $2\theta = 40$, 47, 67 and 83°, corresponding to reflections (1 1 1), (2 0 0), (2 2 0) and (3 1 1), respectively. The reflections from the Ru or RuO_x hcp structure are less intense than those from the Pt-type fcc structure, so the strongest hcp (1 0 1) reflection is obscured by the fcc (1 1 1) reflection. The diffraction peak of alloy particles is typically affected by various parameters, including homogeneity, crystallinity and crystallite

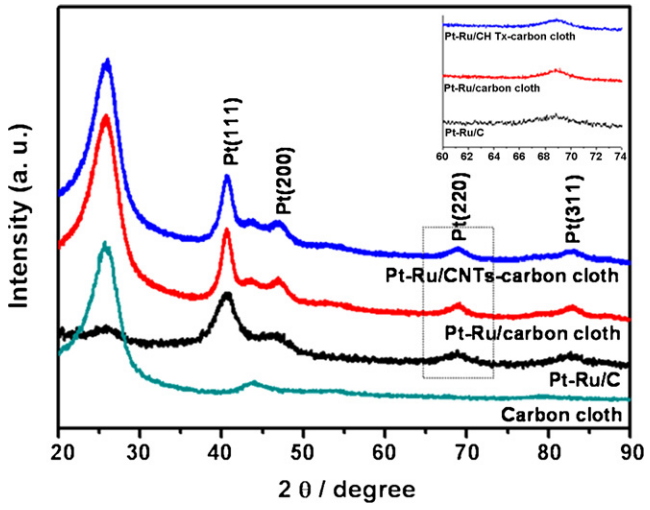

Fig. 6. XRD patterns of Pt-Ru on various electrodes and the background pattern of the carbon cloth; the inset showing Pt-Ru diffraction patterns around fcc (2 2 0).

size. Since fcc (2 2 0) is isolated from graphite diffraction peaks from the carbon support, the diffraction peaks of fcc (2 2 0) of these Pt-Ru electrocatalysts at around 60–74° are presented in the inset of Fig. 6. The fcc (2 2 0) diffraction peak of the Pt–Ru alloy appears between that of Pt fcc (220) (ca. 67.5°) and that of Ru hcp (1 1 0) (ca. 69.4°), and the diffraction angle and full-width at half-maximum (FWHM) of the Pt-Ru fcc (2 2 0) peak are strongly affected by the degree of alloying and the grain size. The diffraction angles of the Pt-Ru/CNTs-CC, the Pt-Ru/CC and the Pt-Ru/XC/CC are 68.80, 68.82 and 68.55°, respectively. Lattice parameters can be evaluated from the angular position of the (2 2 0) peak maxima (θ_{max}), using Vegard's law:

$$a = \frac{\sqrt{2}\lambda_{k\alpha 1}}{\sin\theta_{max}} \quad (3)$$

where $\lambda_{k\alpha 1} = 1.54056$ Å. The Ru atomic fraction in the alloy, x_{Ru}, was determined from XRD data using the formula proposed by Antolini et al. [47]:

$$a = a_0 - 0.124x_{Ru} \quad (4)$$

where a_0 is the lattice parameter of Pt. The degrees of alloying of the Pt-Ru/CNT-CC and the Pt-Ru/CC, x_{Ru}, are 47.74 and 48.54%, respectively. Therefore, these Pt-Ru electrocatalysts, which are prepared by sputtering, appear to form homogeneous alloy nanoclusters. The diffraction angle of the Pt-Ru/XC/CC (ca. 68.55°) is lower than that of the other two samples, suggesting that Pt-Ru/XC/CC exhibits slightly weak alloying (37.80%). The width of the (2 2 0) peak is also selected to estimate the grain size of the Pt-Ru nanoclusters using the Scherrer equation,

$$L = \frac{0.9\lambda_{k\alpha 1}}{B_{(2\theta)}\cos\theta_{max}} \quad (5)$$

where $B_{(2\theta)}$ is the FWHM. The calculated grain sizes in the Pt-Ru/CNTs-CC, the Pt-Ru/CC and the Pt-Ru/XC/CC are 3.90, 3.97 and 3.87 nm, respectively.

Fig. 7 presents CV measurements for the Pt-Ru/CNTs-CC and the Pt-Ru/CC in 1 M methanol solution and 1 M sulfuric acid at a scan rate of 10 mV s^{-1}. The CV feature shows two anodic peaks during scans. An anodic peak during the forward sweep at about 0.55 V is corresponding to the methanol oxidation activity and another anodic peak during the reverse sweep at about 0.45 V is due to the removal of incompletely oxidized carbonaceous species formed in the forward sweep [48]. At a given metal loading of 0.4 mg cm^{-2}, the onset potential of the methanol oxidation of the Pt-Ru/CNTs-CC is lower than that of the Pt-Ru/CC in the anodic sweep, which indicates that the Pt-Ru/CNTs-CC reduces the activation overpotential. The oxidation peaks in anodic sweep are observed at 0.56 and 0.68 V for the Pt-Ru/CNTs-CC and the Pt-Ru/CC, respectively. The oxidation peak of the Pt-Ru/CNTs-CC is more negative, which indicates that the methanol oxidation becomes energetically more favorable. Furthermore, the Pt-Ru/CNTs-CC has a much higher current density after the onset potential, revealing that the current density of the Pt-Ru/CNTs-CC is seven times that of the Pt-Ru/CC at 0.4 V. Guo and Li found that platinum supported on SWNT has a lower onset potential and a higher methanol oxidation current density, which is attributable to the high dispersion of platinum electrocatalysts and various oxide functional groups on the SWNT surface, which serve as "active oxygen" for the formation of CO_2 [26]. In our case, the high performance of the Pt-Ru/CNTs-CC followed not only from the fast electron transport on CNT but also the drop in the interfacial resistance between the CNT and carbon cloth.

Fig. 8 plots the polarization curves of Pt-Ru/CNTs-CC, Pt-Ru/CC and Pt-Ru/XC/CC with metal loadings of 0.4, 0.4 and 3.0 mg cm^{-2}, respectively, as anodes in the DMFC test. The polarization curves of the cells were obtained at 60 °C. At the high cell potential range, the polarization curve is dominated by the activation overpotential, which is directly related to the electrochemical kinetics. A higher metal loading is required to reduce the activation overpotential at the anode; consequently, a higher open-circuit voltage (OCV) is demonstrated with Pt-Ru/XC/CC using a high metal loading. In the middle cell voltage range, the Ohmic overpotential controls the electrochemical reaction. The maximum power densities of the Pt-Ru/CNTs-CC, the Pt-Ru/CC and the Pt-Ru/XC/CC are 73.6, 21.3 and 50.6 mW cm^{-2}, respectively, indicating the improvement in performance associated with the use of a CNTs-carbon

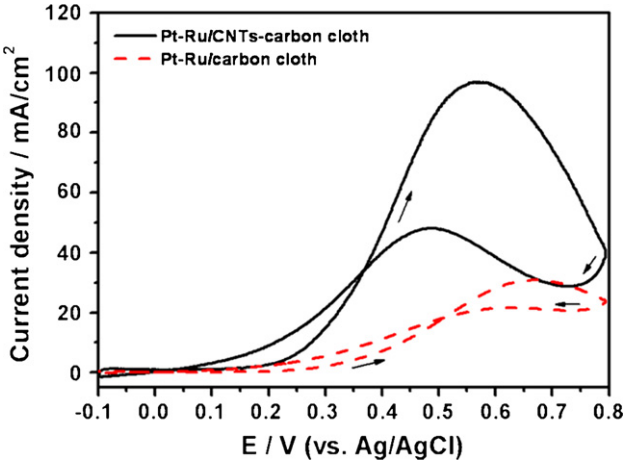

Fig. 7. CV measurements for Pt-Ru on CNTs-carbon cloth electrode and carbon cloth in 1 M methanol/1 M sulfuric acid solution at a scan rate of 10 mV s^{-1}.

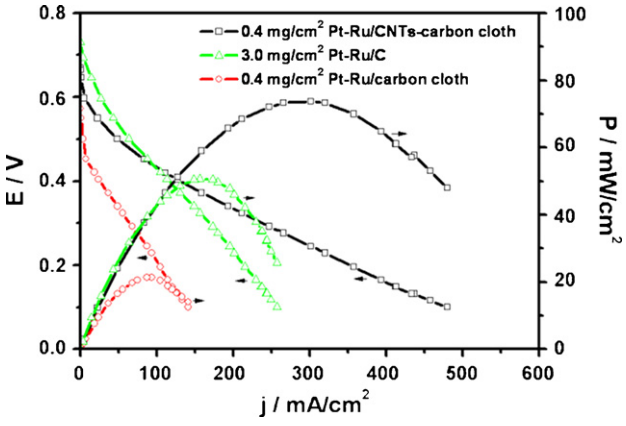

Fig. 8. Polarization curves of DMFCs using various anodes operated at 60 °C with 1 M methanol and oxygen feeding to anode and cathode, respectively.

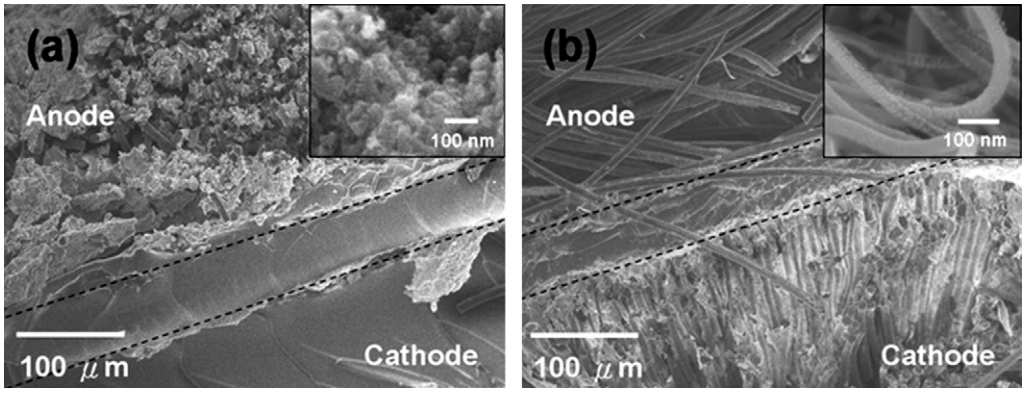

Fig. 9. Cross-sectional HRSEM images of micro-structural MEAs and using (a) Pt-Ru/XC/CC and (b) Pt-Ru/CNTs-CC as anodes.

cloth composite anode in DMFC. At the low cell voltage range, where the mass transport overpotential dominates the reaction, this behavior is not evident herein.

Fig. 9 presents cross-sectional HRSEM images of the micro-structures of MEA. The interfaces between the membrane and the electrodes are marked with dashed lines. The thickness of the electrocatalyst layer depends on numerous factors, such as the total amount of electrocatalyst, the weight percentage of the metal in the electrocatalyst layer, the Nafion ionomer content in the electrocatalyst layer and the method of preparation. The electrocatalyst layer of the anode is typically 50–100 μm thick. Fig. 9(a) presents the micro-structure of MEA, in which the Pt-Ru/XC/CC is used as the anode. However, identifying the boundary between the anodic electrocatalyst layer and the carbon cloth is difficult, because some electrocatalysts were pressed into carbon cloth during hot-pressing. Fig. 9(b) shows that when Pt-Ru/CNTs-CC is used as the anode, the electrocatalyst layer is thinner than 10 μm, and the Pt-Ru nanoclusters were homogenously coated on CNT following hot-pressing, as displayed in the inset in Fig. 9(b). When the conventional screen-printing is adopted, the energy losses are caused by the internal resistances of the activated carbons and interfacial resistances of the contacts between the activated carbons and the carbon cloth. When CNTs-carbon cloth composite is used as the electrode, the electrons from the electrocatalysts are delivered to highly conductive CNT and then directly to the carbon cloth; therefore, energy losses are reduced. Meanwhile, the Pt-Ru/CNTs-CC has a thinner electrocatalyst layer, which results in much efficient electron and proton transport. Both the direct electronic path and thinner electrocatalyst layer contribute to the reduced Ohmic losses in the MEA, which is confirmed in Fig. 8 showing a lower Ohmic overpotential with Pt-Ru/CNTs-CC. The mass transport losses occur in the diffusion of reactants and products through the electrode. A thicker electrocatalyst layer is believed to be associated with greater mass transport losses. A Pt-Ru/CNTs-CC with a thinner electrocatalyst layer is associated with less mass transport loss, which is never observed in Fig. 8.

4. Conclusion

The dispersion and electrochemical characteristics of Pt-Ru nanoclusters on directly grown CNTs have been investigated. The Pt-Ru/CNTs-carbon electrode using a low metal loading of 0.4 mg cm^{-2} exhibits excellent electrochemical activity of methanol oxidation according to CV measurement. It also performs as a superior anode, according to cell measurements. The high performance of the Pt-Ru/CNTs-CC anode is attributable to the smallness of the Pt-Ru particles, the good dispersion of electrocatalysts, the thin electrocatalyst layer, the highly conductive supports, and the low internal and interfacial resistances. Therefore, CNTs directly grown on carbon cloth provides a promising electrocatalytic support for further DMFC.

Acknowledgements

The authors would like to thank the National Science Council and Ministry of Education in Taiwan for financially supporting. Technical assistance from Dr. Cheng-Hsien Hsu (Giant An Technologies Workroom), Mr. Ning-Yih Hsu (Department of Chemical Engineering, National Taiwan University) and Mr. Yao-Sheng Hsu (Asia Pacific Fuel Cell Technologies Ltd.) are gratefully acknowledged.

References

[1] N.A. Hampson, M.J. Willars, B.D. McNicol, J. Power Sources 4 (1979) 191–201.
[2] T. Iwasita, Electrochim. Acta 47 (2002) 3663–3674.
[3] E.A. Batista, G.R.P. Malpass, A.J. Motheo, T. Iwasita, Electrochem. Commun. 5 (2003) 843–846.
[4] F. Barbir, PEM Fuel Cells: Theory and Practice, Elsevier Academic Press, Burlington, MA, 2005, pp. 73–110.
[5] G. Hoogers (Ed.), Fuel Cell Technology Handbook, CRC Press, Boca Raton, FL, 2003, pp. 7-1–7-11.
[6] M. Watanabe, M. Uchida, S. Motoo, J. Electroanal. Chem. 229 (1987) 395–406.
[7] A. Hamnett, Catal. Today 38 (1997) 445–457.
[8] H.A. Gasteiger, N. Markovic, P.N. Ross Jr., E.J. Cairns, J. Phys. Chem. 98 (1994) 617–625.
[9] B. Gurau, R. Viswanathan, T.J. Lafrenz, R. Liu, K.L. Ley, E.S. Smotkin, E. Reddington, A. Sapienza, B.C. Chan, T.E. Mallouk, S. Sarangapani, J. Phys. Chem. B 102 (1998) 9997–10003.
[10] D.R. Rolison, Science 299 (2003) 1698–1701.
[11] C. Lim, C.Y. Wang, J. Power Sources 113 (2003) 145–150.
[12] C.Y. Chen, P. Yang, J. Power Sources 123 (2003) 37–42.
[13] L. Jiang, G. Sun, X. Zhao, Z. Zhou, S. Yan, S. Tang, G. Wang, B. Zhou, Q. Xin, Electrochim. Acta 50 (2005) 2371–2376.
[14] M. Neergat, D. Leveratto, U. Stimming, Fuel Cells 2 (2002) 25–30.

[15] M.P. Hogarth, T.R. Ralph, Platinum Met. Rev. 46 (2002) 146–164.
[16] A.C. Dillon, K.M. Jones, T.A. Bekkedahl, C.H. Kiang, D.S. Bethune, M.J. Heben, Nature 386 (1997) 377–379.
[17] G. Che, B.B. Lakshmi, E.R. Fisher, C.R. Martin, Nature 393 (1998) 346–349.
[18] G.X. Wang, J.-H. Ahn, J. Yao, M. Lindsay, H.K. Liu, S.X. Dou, J. Power Sources 119-121 (2003) 16–23.
[19] K.H. An, W.S. Kim, Y.S. Park, J.-M. Moon, D.J. Bae, S.C. Lim, Y.S. Lee, Y.H. Lee, Adv. Funct. Mater. 11 (2001) 387–392.
[20] W.-C. Fang, J.-H. Huang, C.-L. Sun, L.-C. Chen, P. Papakonstantinou, O.M. Chyan, K.-H. Chen, J. Vac. Sci. Technol. B 24 (2006) 87–90.
[21] W.C. Fang, J.H. Huang, L.C. Chen, Y.O. Su, K.H. Chen, C.L. Sun, Electrochem. Solid-state Lett. 9 (2006) A5–A8.
[22] J. Guo, G. Sun, Q. Wang, G. Wang, Z. Zhou, S. Tang, L. Jiang, B. Zhou, Q. Xin, Carbon 44 (2006) 152–157.
[23] G. Wu, Y.-S. Chen, B.-Q. Xu, Electrochem. Commun. 7 (2005) 1237–1243.
[24] G. Girishkumar, M. Rettker, R. Underhile, D. Binz, K. Vinodgopal, P. McGinn, P. Kamat, Langmuir 21 (2005) 8487–8494.
[25] C. Kim, Y.J. Kim, Y.A. Kim, T. Yanagisawa, K.C. Park, M. Endoa, M.S. Dresselhaus, J. Appl. Phys. 96 (2004) 5903–5905.
[26] D.-J. Guo, H.-L. Li, J. Electroanal. Chem. 573 (2004) 197–202.
[27] C. Wang, M. Waje, X. Wang, J.M. Tang, R.C. Haddon, Y. Yan, Nano Lett. 4 (2004) 345–348.
[28] M. Endo, Y.A. Kim, M. Ezaka, K. Osada, T. Yanagisawa, T. Hayashi, M. Terrones, M.S. Dresselhaus, Nano Lett. 3 (2003) 723–726.
[29] E.S. Steigerwalt, G.A. Deluga, C.M. Lukehart, J. Phys. Chem. B 106 (2002) 760–766.
[30] C.A. Bessel, K. Laubernds, N.M. Rodriguez, R.T.K. Baker, J. Phys. Chem. B 105 (2001) 1115–1118.
[31] M.-C. Tsai, T.-K. Yeh, C.-H. Tsai, Electrochem. Commun. 8 (2006) 1445–1452.
[32] L.-C. Chen, C.-Y. Wen, C.-H. Liang, W.-K. Hong, K.-J. Chen, H.-C. Cheng, C.-S. Shen, C.-T. Wu, K.-H. Chen, Adv. Funct. Mater. 12 (2002) 687–692.
[33] L.H. Chan, K.H. Hong, D.Q. Xiao, T.C. Lin, S.H. Lai, W.J. Hsieh, H.C. Shih, Phys. Rev. B 70 (2004) 125408-1–125408-7.
[34] L.H. Chan, K.H. Hong, D.Q. Xiao, W.J. Hsieh, S.H. Lai, H.C. Shih, T.C. Lin, F.S. Shieu, K.J. Chen, H.C. Cheng, Appl. Phys. Lett. 82 (2003) 4334–4336.
[35] N.S. Kim, Y.T. Lee, J. Park, J.B. Han, Y.S. Choi, S.Y. Choi, J. Choo, G.H. Lee, J. Phys. Chem. B 107 (2003) 9249–9255.
[36] B. Rajesh, V. Karthik, S. Karthikeyan, K. Ravindranathan Thampi, J.-M. Bonard, B. Viswanathan, Fuel 81 (2002) 2177–2190.
[37] C.E. Banks, T.J. Davies, G.G. Wildgoose, R.G. Compton, Chem. Commun. 7 (2005) 829–841.
[38] J.M. Nugent, K.S.V. Santhanam, A. Rubio, P.M. Ajayan, Nano Lett. 1 (2001) 87–91.
[39] L. Chico, L.X. Benedict, S.G. Louie, M.L. Cohen, Phys. Rev. B 54 (1996) 2600–2606.
[40] Yu.V. Pleskov, Yu.E. Evstefeeva, M.D. Krotova, A.V. Laptev, Electrochim. Acta 44 (1999) 3361–3366.
[41] E. Barsoukov, J.R. Macdonald (Eds.), Impedance Spectroscopy Theory, Experiment, and Applications, John Wiley & Sons Inc. Press, Hoboken, NJ, 2005, pp. 430–436.
[42] H. Liu, C. Song, L. Zhang, J. Zhang, H. Wang, D.P. Wilkinson, J. Power Sources 155 (2006) 95–110.
[43] M. Watanabe, S. Motoo, J. Electroanal. Chem. 60 (1975) 267–273.
[44] T. Frelink, W. Visscher, J.A.R. van Veen, Surf. Sci. 335 (1995) 353–360.
[45] C.-L. Sun, L.-C. Chen, M.-C. Su, L.-S. Hong, O. Chyan, C.-Y. Hsu, K.-H. Chen, T.-F. Chang, L. Chang, Chem. Mater. 17 (2005) 3749–3753.
[46] C.-L. Sun, H.-W. Wang, M. Hayashi, L.-C. Chen, K.-H. Chen, J. Am. Chem. Soc. 128 (2006) 8368–8369.
[47] E. Antolini, F. Cardellini, L. Giorgi, E. Passalacqua, J. Mater. Sci. Lett. 19 (2000) 2099–2103.
[48] R. Manoharan, J.B. Goodenough, J. Mater. Chem. 2 (1992) 875–887.